

Observation of $e^+e^- \rightarrow \eta h_c$ at center-of-mass energies from 4.085 to 4.600 GeV

M. Ablikim¹, M. N. Achasov^{9,e}, S. Ahmed¹⁴, O. Albayrak⁵, M. Albrecht⁴,
M. Alekseev^{50A,50C}, A. Amoroso^{50A,50C}, F. F. An¹, Q. An^{47,a}, J. Z. Bai¹, O. Bakina²⁴,
R. Baldini Ferroli^{20A}, Y. Ban³², D. W. Bennett¹⁹, J. V. Bennett⁵, N. Berger²³,
M. Bertani^{20A}, D. Bettoni^{21A}, J. M. Bian⁴⁵, F. Bianchi^{50A,50C}, E. Boger^{24,c}, I. Boyko²⁴,
R. A. Briere⁵, H. Cai⁵², X. Cai^{1,a}, O. Cakir^{42A}, A. Calcaterra^{20A}, G. F. Cao¹,
S. A. Cetin^{42B}, J. Chai^{50C}, J. F. Chang^{1,a}, G. Chelkov^{24,c,d}, G. Chen¹, H. S. Chen¹,
J. C. Chen¹, M. L. Chen^{1,a}, P. L. Chen⁴⁸, S. J. Chen³⁰, X. R. Chen²⁷, Y. B. Chen^{1,a},
X. K. Chu³², G. Cibinetto^{21A}, H. L. Dai^{1,a}, J. P. Dai³⁵, A. Dbeyssi¹⁴, D. Dedovich²⁴,
Z. Y. Deng¹, A. Denig²³, I. Denysenko²⁴, M. Destefanis^{50A,50C}, F. De Mori^{50A,50C},
Y. Ding²⁸, C. Dong³¹, J. Dong^{1,a}, L. Y. Dong¹, M. Y. Dong^{1,a}, O. Dorjkhaidav²²,
Z. L. Dou³⁰, S. X. Du⁵⁴, P. F. Duan¹, J. Fang^{1,a}, S. S. Fang¹, X. Fang^{47,a}, Y. Fang¹,
R. Farinelli^{21A,21B}, L. Fava^{50B,50C}, S. Fegan²³, F. Feldbauer²³, G. Felici^{20A}, C. Q. Feng^{47,a},
E. Fioravanti^{21A}, M. Fritsch^{14,23}, C. D. Fu¹, Gao⁶, Q. Gao¹, X. L. Gao^{47,a}, Y. Gao⁴¹,
Z. Gao^{47,a}, I. Garzia^{21A}, K. Goetzen¹⁰, L. Gong³¹, W. X. Gong^{1,a}, W. Gradl²³,
M. Greco^{50A,50C}, M. H. Gu^{1,a}, S. Gu¹⁵, Y. T. Gu¹², A. Q. Guo¹, L. B. Guo²⁹, R. P. Guo¹,
Y. P. Guo²³, Z. Haddadi²⁶, A. Hafner²³, S. Han⁵², X. Q. Hao¹⁵, F. A. Harris⁴⁴, K. L. He¹,
X. Q. He⁴⁶, F. H. Heinsius⁴, T. Held⁴, Y. K. Heng^{1,a}, T. Holtmann⁴, Z. L. Hou¹, C. Hu²⁹,
H. M. Hu¹, T. Hu^{1,a}, Y. Hu¹, G. S. Huang^{47,a}, J. S. Huang¹⁵, X. T. Huang³⁴,
X. Z. Huang³⁰, Z. L. Huang²⁸, T. Hussain⁴⁹, W. Ikegami Andersson⁵¹, Q. Ji¹, Q. P. Ji¹⁵,
X. B. Ji¹, X. L. Ji^{1,a}, X. S. Jiang^{1,a}, X. Y. Jiang³¹, J. B. Jiao³⁴, Z. Jiao¹⁷, D. P. Jin^{1,a},
S. Jin¹, T. Johansson⁵¹, A. Julin⁴⁵, N. Kalantar-Nayestanaki²⁶, X. L. Kang¹, X. S. Kang³¹,
M. Kavatsyuk²⁶, B. C. Ke⁵, Tabassum Khan Khan^{47,a}, P. Kiese²³, R. Kliemt¹⁰, B. Kloss²³,
L. K. Koch²⁵, O. B. Kolcu^{42B,h}, B. Kopf⁴, M. Kornicer⁴⁴, M. Kuemmel⁴, M. Kuhlmann⁴,
A. Kupsc⁵¹, W. Kühn²⁵, J. S. Lange²⁵, M. Lara¹⁹, P. Larin¹⁴, L. Lavezzi^{50C,1}, H. Leithoff²³,
C. Leng^{50C}, C. Li⁵¹, Cheng Li^{47,a}, D. M. Li⁵⁴, F. Li^{1,a}, F. Y. Li³², G. Li¹, H. B. Li¹,
H. J. Li¹, J. C. Li¹, Jin Li³³, K. Li¹³, K. Li³⁴, Lei Li³, P. L. Li^{47,a}, P. R. Li^{7,43}, Q. Y. Li³⁴,
T. Li³⁴, W. D. Li¹, W. G. Li¹, X. L. Li³⁴, X. N. Li^{1,a}, X. Q. Li³¹, Z. B. Li⁴⁰, H. Liang^{47,a},
Y. F. Liang³⁷, Y. T. Liang²⁵, G. R. Liao¹¹, D. X. Lin¹⁴, B. Liu³⁵, B. J. Liu¹, C. X. Liu¹,
D. Liu^{47,a}, F. H. Liu³⁶, Fang Liu¹, Feng Liu⁶, H. B. Liu¹², H. H. Liu¹, H. H. Liu¹⁶,
H. M. Liu¹, J. B. Liu^{47,a}, J. P. Liu⁵², J. Y. Liu¹, K. Liu⁴¹, K. Y. Liu²⁸, Ke Liu⁶,
L. D. Liu³², P. L. Liu^{1,a}, Q. Liu⁴³, S. B. Liu^{47,a}, X. Liu²⁷, Y. B. Liu³¹, Y. Y. Liu³¹,
Z. A. Liu^{1,a}, Zhiqing Liu²³, Y. F. Long³², X. C. Lou^{1,a,g}, H. J. Lu¹⁷, J. G. Lu^{1,a}, Y. Lu¹,
Y. P. Lu^{1,a}, C. L. Luo²⁹, M. X. Luo⁵³, T. Luo⁴⁴, X. L. Luo^{1,a}, X. R. Lyu⁴³, F. C. Ma²⁸,
H. L. Ma¹, L. L. Ma³⁴, M. M. Ma¹, Q. M. Ma¹, T. Ma¹, X. N. Ma³¹, X. Y. Ma^{1,a},
Y. M. Ma³⁴, F. E. Maas¹⁴, M. Maggiora^{50A,50C}, Q. A. Malik⁴⁹, Y. J. Mao³², Z. P. Mao¹,
S. Marcello^{50A,50C}, J. G. Messchendorp²⁶, G. Mezzadri^{21B}, J. Min^{1,a}, T. J. Min¹,
R. E. Mitchell¹⁹, X. H. Mo^{1,a}, Y. J. Mo⁶, C. Morales Morales¹⁴, G. Morello^{20A},
N. Yu. Muchnoi^{9,e}, H. Muramatsu⁴⁵, P. Musiol⁴, A. Mustafa⁴, Y. Nefedov²⁴, F. Nerling¹⁰,
I. B. Nikolaev^{9,e}, Z. Ning^{1,a}, S. Nisar⁸, S. L. Niu^{1,a}, X. Y. Niu¹, S. L. Olsen³³, Q. Ouyang^{1,a},
S. Pacetti^{20B}, Y. Pan^{47,a}, P. Patteri^{20A}, M. Pelizaeus⁴, J. Pellegrino^{50A,50C}, H. P. Peng^{47,a},
K. Peters^{10,i}, J. Pettersson⁵¹, J. L. Ping²⁹, R. G. Ping¹, R. Poling⁴⁵, V. Prasad^{39,47},

H. R. Qi², M. Qi³⁰, S. Qian^{1,a}, C. F. Qiao⁴³, J. J. Qin⁴³, N. Qin⁵², X. S. Qin¹,
Z. H. Qin^{1,a}, J. F. Qiu¹, K. H. Rashid⁴⁹, C. F. Redmer²³, M. Richter⁴, M. Ripka²³,
G. Rong¹, Ch. Rosner¹⁴, X. D. Ruan¹², A. Sarantsev^{24,f}, M. Savrie^{21B}, C. Schnier⁴,
K. Schoenning⁵¹, W. Shan³², M. Shao^{47,a}, C. P. Shen², P. X. Shen³¹, X. Y. Shen¹,
H. Y. Sheng¹, J. J. Song³⁴, X. Y. Song¹, S. Sosio^{50A,50C}, C. Sowa⁴, S. Spataro^{50A,50C},
G. X. Sun¹, J. F. Sun¹⁵, S. S. Sun¹, X. H. Sun¹, Y. J. Sun^{47,a}, Y. K. Sun^{47,a}, Y. Z. Sun¹,
Z. J. Sun^{1,a}, Z. T. Sun¹⁹, C. J. Tang³⁷, X. Tang¹, I. Tapan^{42C}, M. Tiemens²⁶, Ts Tsednee²²,
I. Uman^{42D}, G. S. Varner⁴⁴, B. Wang¹, B. L. Wang⁴³, D. Wang³², D. Y. Wang³²,
Dan Wang⁴³, K. Wang^{1,a}, L. L. Wang¹, L. S. Wang¹, M. Wang³⁴, P. Wang¹, P. L. Wang¹,
W. P. Wang^{47,a}, X. F. Wang⁴¹, Y. D. Wang¹⁴, Y. F. Wang^{1,a}, Y. Q. Wang²³, Z. Wang^{1,a},
Z. G. Wang^{1,a}, Z. H. Wang^{47,a}, Z. Y. Wang¹, Z. Y. Wang¹, T. Weber²³, D. H. Wei¹¹,
P. Weidenkaff²³, S. P. Wen¹, U. Wiedner⁴, M. Wolke⁵¹, L. H. Wu¹, L. J. Wu¹, Z. Wu^{1,a},
L. Xia^{47,a}, Y. Xia¹⁸, D. Xiao¹, Y. J. Xiao¹, Z. J. Xiao²⁹, Y. G. Xie^{1,a}, Yuehong Xie⁶,
X. A. Xiong¹, Q. L. Xiu^{1,a}, G. F. Xu¹, J. J. Xu¹, L. Xu¹, Q. J. Xu¹³, Q. N. Xu⁴³,
X. P. Xu³⁸, L. Yan^{50A,50C}, W. B. Yan^{47,a}, W. C. Yan^{47,a}, Y. H. Yan¹⁸, H. J. Yang^{35,j},
H. X. Yang¹, L. Yang⁵², Y. H. Yang³⁰, Y. X. Yang¹¹, M. Ye^{1,a}, M. H. Ye⁷, J. H. Yin¹,
Z. Y. You⁴⁰, B. X. Yu^{1,a}, C. X. Yu³¹, J. S. Yu²⁷, C. Z. Yuan¹, Y. Yuan¹, A. Yuncu^{42B,b},
A. A. Zafar⁴⁹, Y. Zeng¹⁸, Z. Zeng^{47,a}, B. X. Zhang¹, B. Y. Zhang^{1,a}, C. C. Zhang¹,
D. H. Zhang¹, H. H. Zhang⁴⁰, H. Y. Zhang^{1,a}, J. Zhang¹, J. L. Zhang¹, J. Q. Zhang¹,
J. W. Zhang^{1,a}, J. Y. Zhang¹, J. Z. Zhang¹, K. Zhang¹, L. Zhang⁴¹, S. Q. Zhang³¹,
X. Y. Zhang³⁴, Y. Zhang¹, Y. Zhang¹, Y. H. Zhang^{1,a}, Y. T. Zhang^{47,a}, Yu Zhang⁴³,
Z. H. Zhang⁶, Z. P. Zhang⁴⁷, Z. Y. Zhang⁵², G. Zhao¹, J. W. Zhao^{1,a}, J. Y. Zhao¹,
J. Z. Zhao^{1,a}, Lei Zhao^{47,a}, Ling Zhao¹, M. G. Zhao³¹, Q. Zhao¹, S. J. Zhao⁵⁴, T. C. Zhao¹,
Y. B. Zhao^{1,a}, Z. G. Zhao^{47,a}, A. Zhemchugov^{24,c}, B. Zheng⁴⁸, J. P. Zheng^{1,a}, W. J. Zheng³⁴,
Y. H. Zheng⁴³, B. Zhong²⁹, L. Zhou^{1,a}, X. Zhou⁵², X. K. Zhou^{47,a}, X. R. Zhou^{47,a},
X. Y. Zhou¹, Y. X. Zhou^{12,a}, K. Zhu¹, K. J. Zhu^{1,a}, S. Zhu¹, S. H. Zhu⁴⁶, X. L. Zhu⁴¹,
Y. C. Zhu^{47,a}, Y. S. Zhu¹, Z. A. Zhu¹, J. Zhuang^{1,a}, L. Zotti^{50A,50C}, B. S. Zou¹, J. H. Zou¹.

(BESIII Collaboration)

¹ *Institute of High Energy Physics, Beijing 100049, People's Republic of China*

² *Beihang University, Beijing 100191, People's Republic of China*

³ *Beijing Institute of Petrochemical Technology, Beijing 102617, People's Republic of China*

⁴ *Bochum Ruhr-University, D-44780 Bochum, Germany*

⁵ *Carnegie Mellon University, Pittsburgh, Pennsylvania 15213, USA*

⁶ *Central China Normal University, Wuhan 430079, People's Republic of China*

⁷ *China Center of Advanced Science and Technology,
Beijing 100190, People's Republic of China*

⁸ *COMSATS Institute of Information Technology, Lahore,
Defence Road, Off Raiwind Road, 54000 Lahore, Pakistan*

⁹ *G.I. Budker Institute of Nuclear Physics SB RAS (BINP), Novosibirsk 630090, Russia*

¹⁰ *GSI Helmholtzcentre for Heavy Ion Research GmbH, D-64291 Darmstadt, Germany*

¹¹ *Guangxi Normal University, Guilin 541004, People's Republic of China*

¹² *Guangxi University, Nanning 530004, People's Republic of China*

¹³ *Hangzhou Normal University, Hangzhou 310036, People's Republic of China*

- ¹⁴ *Helmholtz Institute Mainz, Johann-Joachim-Becher-Weg 45, D-55099 Mainz, Germany*
- ¹⁵ *Henan Normal University, Xinxiang 453007, People's Republic of China*
- ¹⁶ *Henan University of Science and Technology, Luoyang 471003, People's Republic of China*
- ¹⁷ *Huangshan College, Huangshan 245000, People's Republic of China*
- ¹⁸ *Hunan University, Changsha 410082, People's Republic of China*
- ¹⁹ *Indiana University, Bloomington, Indiana 47405, USA*
- ²⁰ *(A)INFN Laboratori Nazionali di Frascati, I-00044, Frascati, Italy; (B)INFN and University of Perugia, I-06100, Perugia, Italy*
- ²¹ *(A)INFN Sezione di Ferrara, I-44122, Ferrara, Italy; (B)University of Ferrara, I-44122, Ferrara, Italy*
- ²² *Institute of Physics and Technology, Peace Ave. 54B, Ulaanbaatar 13330, Mongolia*
- ²³ *Johannes Gutenberg University of Mainz, Johann-Joachim-Becher-Weg 45, D-55099 Mainz, Germany*
- ²⁴ *Joint Institute for Nuclear Research, 141980 Dubna, Moscow region, Russia*
- ²⁵ *Justus-Liebig-Universitaet Giessen, II. Physikalisches Institut, Heinrich-Buff-Ring 16, D-35392 Giessen, Germany*
- ²⁶ *KVI-CART, University of Groningen, NL-9747 AA Groningen, The Netherlands*
- ²⁷ *Lanzhou University, Lanzhou 730000, People's Republic of China*
- ²⁸ *Liaoning University, Shenyang 110036, People's Republic of China*
- ²⁹ *Nanjing Normal University, Nanjing 210023, People's Republic of China*
- ³⁰ *Nanjing University, Nanjing 210093, People's Republic of China*
- ³¹ *Nankai University, Tianjin 300071, People's Republic of China*
- ³² *Peking University, Beijing 100871, People's Republic of China*
- ³³ *Seoul National University, Seoul, 151-747 Korea*
- ³⁴ *Shandong University, Jinan 250100, People's Republic of China*
- ³⁵ *Shanghai Jiao Tong University, Shanghai 200240, People's Republic of China*
- ³⁶ *Shanxi University, Taiyuan 030006, People's Republic of China*
- ³⁷ *Sichuan University, Chengdu 610064, People's Republic of China*
- ³⁸ *Soochow University, Suzhou 215006, People's Republic of China*
- ³⁹ *State Key Laboratory of Particle Detection and Electronics, Beijing 100049, Hefei 230026, People's Republic of China*
- ⁴⁰ *Sun Yat-Sen University, Guangzhou 510275, People's Republic of China*
- ⁴¹ *Tsinghua University, Beijing 100084, People's Republic of China*
- ⁴² *(A)Ankara University, 06100 Tandogan, Ankara, Turkey; (B)Istanbul Bilgi University, 34060 Eyup, Istanbul, Turkey; (C)Uludag University, 16059 Bursa, Turkey; (D)Near East University, Nicosia, North Cyprus, Mersin 10, Turkey*
- ⁴³ *University of Chinese Academy of Sciences, Beijing 100049, People's Republic of China*
- ⁴⁴ *University of Hawaii, Honolulu, Hawaii 96822, USA*
- ⁴⁵ *University of Minnesota, Minneapolis, Minnesota 55455, USA*
- ⁴⁶ *University of Science and Technology Liaoning, Anshan 114051, People's Republic of China*
- ⁴⁷ *University of Science and Technology of China, Hefei 230026, People's Republic of China*
- ⁴⁸ *University of South China, Hengyang 421001, People's Republic of China*
- ⁴⁹ *University of the Punjab, Lahore-54590, Pakistan*

⁵⁰ (A) *University of Turin, I-10125, Turin, Italy; (B) University of Eastern Piedmont, I-15121, Alessandria, Italy; (C) INFN, I-10125, Turin, Italy*

⁵¹ *Uppsala University, Box 516, SE-75120 Uppsala, Sweden*

⁵² *Wuhan University, Wuhan 430072, People's Republic of China*

⁵³ *Zhejiang University, Hangzhou 310027, People's Republic of China*

⁵⁴ *Zhengzhou University, Zhengzhou 450001, People's Republic of China*

^a *Also at State Key Laboratory of Particle Detection and Electronics, Beijing 100049, Hefei 230026, People's Republic of China*

^b *Also at Bogazici University, 34342 Istanbul, Turkey*

^c *Also at the Moscow Institute of Physics and Technology, Moscow 141700, Russia*

^d *Also at the Functional Electronics Laboratory, Tomsk State University, Tomsk, 634050, Russia*

^e *Also at the Novosibirsk State University, Novosibirsk, 630090, Russia*

^f *Also at the NRC "Kurchatov Institute", PNPI, 188300, Gatchina, Russia*

^g *Also at University of Texas at Dallas, Richardson, Texas 75083, USA*

^h *Also at Istanbul Arel University, 34295 Istanbul, Turkey*

ⁱ *Also at Goethe University Frankfurt, 60323 Frankfurt am Main, Germany*

^j *Also at Institute of Nuclear and Particle Physics, Shanghai Key Laboratory for Particle Physics and Cosmology, Shanghai 200240, People's Republic of China*

(Dated: May 18, 2019)

Abstract

We observe for the first time the process $e^+e^- \rightarrow \eta h_c$ with data collected by the BESIII experiment. Significant signals are observed at the center-of-mass energy $\sqrt{s} = 4.226$ GeV, and the Born cross section is measured to be $(9.5_{-2.0}^{+2.2} \pm 2.7)$ pb. Evidence for ηh_c is observed at $\sqrt{s} = 4.358$ GeV with a Born cross section of $(10.0_{-2.7}^{+3.1} \pm 2.6)$ pb, and upper limits on the production cross section at other center-of-mass energies between 4.085 and 4.600 GeV are determined.

PACS numbers: 13.25.Gv, 13.66.Bc, 14.40.Pq, 14.40.Rt

I. INTRODUCTION

The spectroscopy of charmonium states below the open charm threshold is well established, but the situation above the threshold is more complicated. From the inclusive hadronic cross section in e^+e^- annihilation, some vector charmonium states, $\psi(3770)$, $\psi(4040)$, $\psi(4160)$, $\psi(4415)$ are known with properties as expected in the quark model [1]. However, besides these states, several new vector states, namely the Y(4260), Y(4360) and Y(4660), have been discovered experimentally [2–7]. In addition, some new states with other quantum number configurations are also found in ex-

periment, such as the $X(3872)$, $Z_c(3900)$ and $Z_c(4020)$ states [5, 8–16]. The common properties of these states are their relatively narrow width for decaying into a pair of charmed mesons, and their strong coupling to hidden charm final states. Therefore, it is hard to explain all these resonances as charmonia and they are named ‘charmonium-like states’ collectively. Several unconventional explanations, such as hybrid charmonium [17, 18], tetraquark [19–21], hadronic molecule [22–24], diquarks [25, 26] or kinematical effects [27–30] have been suggested. See also Ref. [31, 32] and references therein for a recent review.

To understand the nature of these

charmonium-like states, it is mandatory to investigate both open and hidden charm decays. Most of the observed vector charmonium-like states transit to spin-triplet charmonium states with large rate since the spin alignment of the c and \bar{c} -quarks does not need to be changed between initial and final states. However, the spin-flip process $e^+e^- \rightarrow \pi\pi h_c$ has also been observed by the CLEO [33] and BESIII experiments [13, 15], and the large cross section exceeds theoretical expectations [34]. Furthermore, two new structures have been reported in $e^+e^- \rightarrow \pi^+\pi^-h_c$ [35]. This may suggest the existence of hybrid charmonium states with a pair of $c\bar{c}$ in spin-singlet configuration which easily couples to an h_c final state. Consequently, searching for the process $e^+e^- \rightarrow \eta h_c$ is necessary. On the one hand, it will provide more information about the spin-flip transition, and the structures observed in $e^+e^- \rightarrow \pi\pi h_c$ are expected to be found also in the ηh_c process. On the other hand, the transition $\Upsilon(4S) \rightarrow \eta h_b$ has been observed in the bottomonium system [36]. Therefore, a search for the production mechanism of the analogous process in the charmonium system is interesting.

The CLEO Collaboration observed evidence of about 3σ for $e^+e^- \rightarrow \eta h_c$ based on 586 pb^{-1} data taken at $\sqrt{s} = 4.17 \text{ GeV}$ [33], and the measured cross section is $(4.7 \pm 2.2) \text{ pb}$. In comparison, BESIII has collected data samples of about 4.7 fb^{-1} in total at $\sqrt{s} > 4.0 \text{ GeV}$. In this paper, a search is performed for the process $e^+e^- \rightarrow \eta h_c$ with $h_c \rightarrow \gamma\eta_c$ based on data samples collected with the BESIII detector at center-of-mass (c.m.) energies from 4.085 to 4.600 GeV, as listed in Table I. The integrated luminosities of these data samples are measured by analyzing large-angle Bhabha scattering events with an uncertainty of 1.0% [37], and the c.m. energies are measured using the di-muon process [38]. In the analysis, η_c is reconstructed with 16 hadronic final states: $p\bar{p}$,

$2(\pi^+\pi^-)$, $2(K^+K^-)$, $K^+K^-\pi^+\pi^-$, $p\bar{p}\pi^+\pi^-$, $3(\pi^+\pi^-)$, $K^+K^-2(\pi^+\pi^-)$, $K^+K^-\pi^0$, $p\bar{p}\pi^0$, $K_S^0K^\pm\pi^\mp$, $K_S^0K^\pm\pi^\mp\pi^\pm\pi^\mp$, $\pi^+\pi^-\eta$, $K^+K^-\eta$, $2(\pi^+\pi^-\eta)$, $\pi^+\pi^-\pi^0\pi^0$, and $2(\pi^+\pi^-\pi^0\pi^0)$, in which K_S^0 is reconstructed from its $\pi^+\pi^-$ decay, and π^0 and η from their $\gamma\gamma$ final state.

II. DETECTOR AND DATA SAMPLES

BEPCCII is a two-ring e^+e^- collider designed for a peak luminosity of $10^{33} \text{ cm}^{-2}\text{s}^{-1}$ at a beam current of 0.93 A per beam. The cylindrical core of the BESIII detector consists of a helium-gas-based main drift chamber (MDC) for charged-particle tracking and particle identification (PID) through the specific energy loss dE/dx , a plastic scintillator time-of-flight (TOF) system for additional PID, and a 6240-crystal CsI(Tl) electromagnetic calorimeter (EMC) for electron identification and photon detection. These components are all enclosed in a superconducting solenoidal magnet providing a 1-T magnetic field. The solenoid is supported by an octagonal flux-return yoke instrumented with resistive-plate-counter muon detector modules interleaved with steel. The geometrical acceptance for charged tracks and photons is 93% of 4π , and the resolutions for charged-track momentum at 1 GeV is 0.5%. The resolutions of photon energy in barrel and end-cap regions are 2.5% and 5%, respectively. More details on the features and capabilities of BESIII are provided in Ref. [39].

A Monte Carlo (MC) simulation is used to determine the detection efficiency and to estimate physics background. The detector response is modelled with a GEANT4-based [40, 41] detector simulation package. Signal and background processes are generated with specialized models that have been packaged and customized for BESIII. 40,000 MC events are generated for each decay mode of η_c at each c.m. energy with KKMC [42] and BESEVTGEN [43]. The

events are generated with an h_c mass of $3525.28 \text{ MeV}/c^2$ and a width of 1.0 MeV . The $E1$ transition $h_c \rightarrow \gamma\eta_c$ is generated with an angular distribution of $1 + \cos^2\theta^*$, where θ^* is the angle of the $E1$ photon with respect to the h_c helicity direction in the h_c rest frame. Multi-body η_c decays are generated uniformly in phase space. In order to study potential backgrounds, inclusive MC samples are produced at $\sqrt{s} = 4.23, 4.26$ and 4.36 GeV corresponding to integrated luminosity of 1000 pb^{-1} , 500 pb^{-1} and 500 pb^{-1} , respectively. They are generated using KKMC, which includes the decay of $Y(4260)$, ISR production of the vector charmonium states, charmed meson production, QED events, and continuum processes. The known decay modes of the resonances are generated with BESEVTGEN with branching fractions set to the world average values [44]. The remaining charmonium decays are generated with LUNDCHARM [45], while other hadronic events are generated with PYTHIA [46].

III. EVENT SELECTION AND STUDY OF BACKGROUND

According to the MC simulation of $e^+e^- \rightarrow \eta h_c$ with $h_c \rightarrow \gamma\eta_c$ at $\sqrt{s} = 4.226 \text{ GeV}$, the energy of the photon emitted in the $E1$ transition $h_c \rightarrow \gamma\eta_c$ is expected to be in the range $(400, 600) \text{ MeV}$ in the laboratory frame. Therefore, the signal event should have one $E1$ photon candidate with energy located in the expected region and one η candidate with recoil mass in the region of $(3480, 3600) \text{ MeV}/c^2$. We define the η recoil mass $M_{\text{recoil}}(\eta)$ as $M_{\text{recoil}}(\eta)^2 c^4 \equiv (E_{\text{cm}} - E_\eta)^2 - |\vec{p}_{\text{cm}} - \vec{p}_\eta|^2 c^2$, where $(E_{\text{cm}}, \vec{p}_{\text{cm}})$ and (E_η, \vec{p}_η) are the four-momenta of the e^+e^- system and η in the e^+e^- rest frame. Since the $E1$ photon energy distribution in the laboratory frame will broaden with increasing c.m. energy, the energy window requirement is enlarged to $(350, 650) \text{ MeV}$ for the data sets collected at $\sqrt{s} > 4.416 \text{ GeV}$.

The η_c candidate is reconstructed by the hadronic systems determined by the corresponding decay mode. The invariant mass of the hadronic systems is required to be within the mass range of $(2940, 3020) \text{ MeV}/c^2$. For the selected candidates, we apply a fit to the distribution of the η recoil mass to obtain the signal yield.

Charged tracks in BESIII are reconstructed from MDC hits within a fiducial range of $|\cos\theta| < 0.93$, where θ is the polar angle of the track. We require that the point of closest approach (POCA) to the interaction point (IP) is within 10 cm in the beam direction and within 1 cm in the plane perpendicular to the beam direction. A vertex fit constrains the production vertex, which is determined run by run, and all the charged tracks to a common vertex. Since the K_S^0 has a relatively long lifetime, it will travel a certain distance in the detector to the point where it decays into daughter particles. The requirements on the track POCA and the vertex fit mentioned above are therefore not applied to its daughter particles. The TOF and dE/dx information are combined to form PID confidence levels (C.L.) for the pion, kaon, and proton hypotheses; both PID and kinematic fit information is used to determine the particle type of each charged track, as discussed below.

Electromagnetic showers are reconstructed by clustering EMC crystal energies. Efficiency and energy resolution are improved by including energy deposits in nearby TOF counters. A photon candidate is defined by showers detected with the EMC exceeding a threshold of 25 MeV in the barrel region ($|\cos\theta| < 0.8$) or of 50 MeV in the end-cap region ($0.86 < |\cos\theta| < 0.92$). Showers in the transition region between the barrel and the end-cap are excluded because of the poor reconstruction. Moreover, EMC cluster timing requirements are used to suppress electronic noise and energy deposits unrelated to the event.

Candidates for π^0 (η) mesons are reconstructed from pairs of photons with an in-

variant mass $M(\gamma\gamma)$ satisfying $|M(\gamma\gamma) - m_{\pi^0(\eta)}| < 15 \text{ MeV}/c^2$. A one-constraint (1C) kinematic fit with the $M(\gamma\gamma)$ constrained to the π^0 (η) nominal mass m_{π^0} (m_η) [44] is performed to improve the energy resolution. We reconstruct $K_S^0 \rightarrow \pi^+\pi^-$ candidates with pairs of oppositely charged tracks with an invariant mass in the mass range of $|M(\pi\pi) - m_{K_S}| < 20 \text{ MeV}/c^2$. Here, m_{K_S} denotes the nominal mass of K_S^0 [44]. A vertex fit constrains the charged tracks to a common decay vertex, and the corrected track parameters are used to calculate the invariant mass. To reject random $\pi^+\pi^-$ combinations, a kinematic constraint between the production and decay vertices, called a secondary-vertex fit, is employed [47], and the decay length is required to be more than twice the vertex resolution.

The η_c candidate is reconstructed in its decay to one of the 16 decay modes mentioned earlier. After the above selection, a four-constraint (4C) kinematic fit is performed for each event imposing overall energy-momentum conservation, and the χ_{4C}^2 is required to be less than 25 to suppress background events with different final states. If multiple η_c candidates are found in an event, only the one with the smallest $\chi^2 \equiv \chi_{4C}^2 + \chi_{1C}^2 + \chi_{\text{pid}}^2 + \chi_{\text{vertex}}^2$ is retained, where χ_{1C}^2 is the χ^2 of the 1C fit for π^0 (η), χ_{pid}^2 is the sum over all charged tracks of the χ^2 of the PID hypotheses, and χ_{vertex}^2 is the χ^2 of the K_S^0 secondary-vertex fit. If more than one η candidate with recoil mass in the h_c signal region ($3480 < M_{\text{recoil}}(\eta) < 3600 \text{ MeV}/c^2$) is found, the one which leads to a mass of the η_c candidate closest to the η_c nominal mass m_{η_c} is selected to reconstruct the η_c .

The requirement on χ_{4C}^2 and mass (energy) windows for η , η_c and $E1$ photon reconstruction are determined by maximizing the figure-of-merit, $\text{FOM} = N_S/\sqrt{N_S + N_B}$, where N_S represents the number of signal events determined by MC simulation, and N_B represents the number of background

events obtained from h_c sidebands in the data sample. The cross section of $e^+e^- \rightarrow \eta h_c$ measured by CLEO [33] and the η_c branching ratios given by the Particle Data Group (PDG) [44] are used to scale the number of signal events in the optimization.

After applying all the criteria to the data sample taken at $\sqrt{s} = 4.226 \text{ GeV}$, the events cluster in the signal region in the two-dimensional distribution as shown in Fig. 1(a). If the two-dimensional histogram is projected to each axis, clear η_c and h_c signals can be found in the expected regions as shown in Fig. 1(b) and (c). Meanwhile, no structure is observed in the events from the η_c (h_c) sideband regions. To further understand the background shape, events located in the η sideband regions are also investigated, which are shown by the green shaded area in Fig. 1 (d) and are well described by a smooth distribution.

In addition, inclusive MC samples generated at $\sqrt{s} = 4.23 \text{ GeV}$ are analyzed to study the background components. Here, the ratios among different components are fixed according to theoretical calculation or experimental measurements, except for the Bhabha process. A sample of 1.0×10^7 Bhabha events (about 2% of the Bhabha events in real data) is generated with the BABAYAGA generator [48] for background estimation. From this study, the dominant background sources are found to be continuum processes according to the MC truth information, while $Y(4260)$ decays only give a small contribution to the total background. Most background events from resonance decays are $\pi\pi J/\psi$, $\omega\chi_{c0}$ and open charm production. A similar conclusion can be drawn for data samples taken at other c.m. energies. From the study above, we conclude that the background shape in the η recoil mass can be described by a linear function.

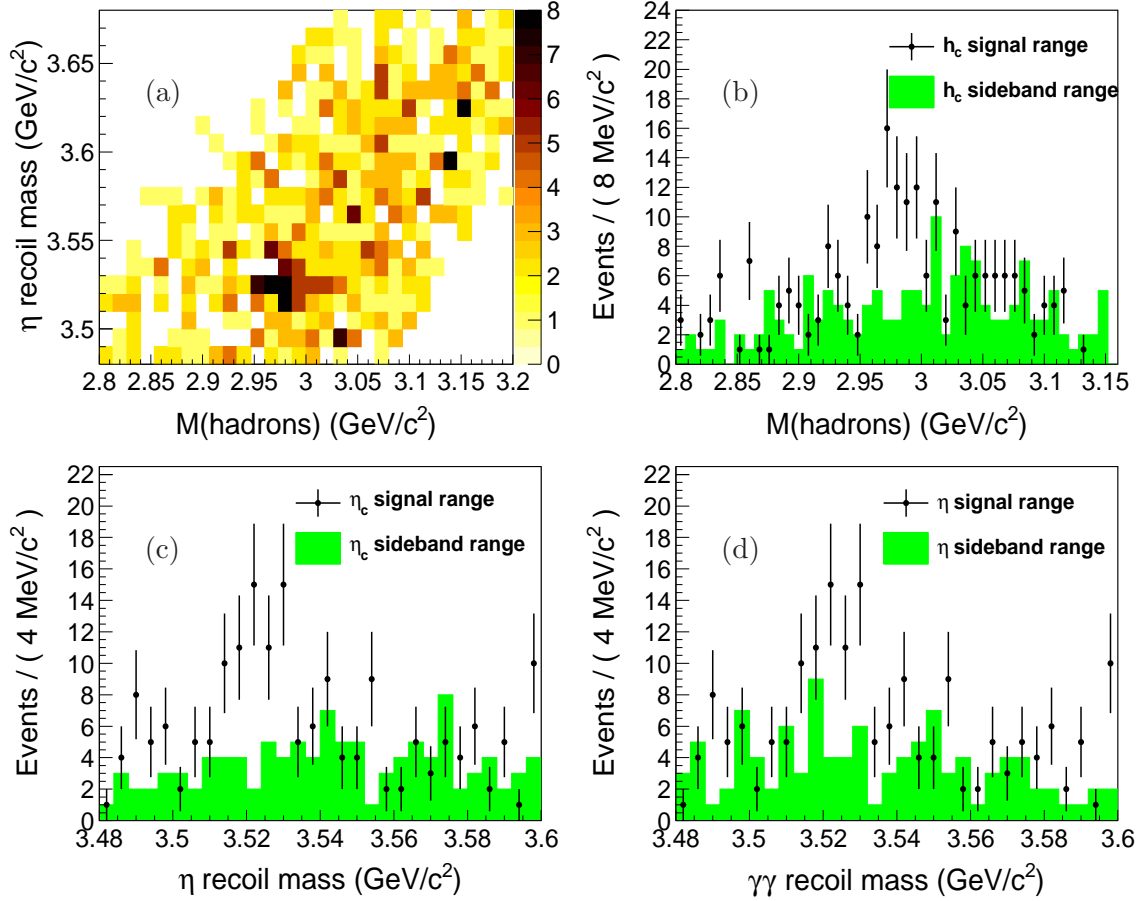


FIG. 1: Mass spectrum obtained at $\sqrt{s} = 4.226$ GeV. (a) The two-dimensional distribution of the invariant mass of the hadronic system and the recoil mass of η ; (b) mass of hadrons in h_c signal ($[3.51, 3.55]$ GeV/c²) and sideband regions ($[3.48, 3.50]$ GeV/c² and $[3.56, 3.58]$ GeV/c²); (c) η recoil mass in η_c signal ($[2.94, 3.02]$ GeV/c²) and sideband region ($[2.87, 2.91]$ GeV/c² and $[3.05, 3.09]$ GeV/c²), and (d) $\gamma\gamma$ recoil mass in η signal ($[0.531, 0.563]$ GeV/c²) and sideband regions ($[0.505, 0.521]$ GeV/c² and $[0.573, 0.589]$ GeV/c²). For (b), (c), and (d), the dots with error bars represent the distributions in the signal regions and the shaded histograms represent the distributions in the sidebands.

IV. FIT TO THE RECOIL MASS OF η

To obtain the h_c yield for each η_c decay channel, the 16 η recoil mass distributions are fitted simultaneously using an unbinned maximum likelihood method. In the fit, the signal shape is determined by the MC simulation and the background shape is described by a linear function. The total signal yield of 16 channels is set to be N_{obs} , which is

the common variable for all sub-samples and required to be positive. $N_{\text{obs}} \times f_i$ is the signal yield of the i -th channel. Here, f_i refers to the weight factor $f_i \equiv \mathcal{B}_i \epsilon_i / \sum \epsilon_i \mathcal{B}_i$, in which the \mathcal{B}_i denotes the branching fraction of η_c decays to the i -th final state and ϵ_i represents the corresponding efficiency. The efficiency for two-body η_c decays is about 20%, for three- or four-body decays is about 10% and for six-body decays it is about 6%. The signal and the background normaliza-

tion for each mode are free parameters in the fit. The mode-by-mode and summed fit results are shown in Figs. 2 and 3, respectively. The χ^2 per degree of freedom (dof) for this fit is $\chi^2/\text{dof} = 17.2/15 = 1.15$, where sparsely populated bins are combined so that there are at least 7 counts per bin in the χ^2 calculation. The total signal yield is

41 ± 9 with a statistical significance of 5.8σ .

With the same method, evidence for $e^+e^- \rightarrow \eta h_c$ is found in the data sample taken at $\sqrt{s} = 4.358 \text{ GeV}$, as shown in Fig. 4, but no obvious signals are observed for the data sets taken at other c.m. energies.

V. BORN CROSS SECTION MEASUREMENT

The Born cross section is calculated using the following formula:

$$\sigma^{\text{Born}}(e^+e^- \rightarrow \eta h_c) = \frac{N_{\text{obs}}}{\mathcal{L}(1 + \delta) |1 + \Pi|^2 \mathcal{B}(\eta \rightarrow \gamma\gamma) \mathcal{B}(h_c \rightarrow \gamma\eta_c) \sum_i \epsilon_i \mathcal{B}_i}. \quad (1)$$

Here, \mathcal{L} is the integrated luminosity of the data sample taken at each c.m. energy. $(1 + \delta)$ is the radiative correction factor, which is defined as

$$(1 + \delta) = \frac{\int \sigma(s(1-x)) F(x, s) dx}{\sigma(s)}, \quad (2)$$

where $F(x, s)$ is the radiator function, which is known from a QED calculation with an accuracy of 0.1% [49], and $\sigma(s)$ is the energy dependent Born cross section in the range of [4.07, 4.6] GeV. Actually, the radiative correction depends on the Born cross section from the production threshold to the e^+e^- collision energy, which is also what we want to measure in this analysis. Therefore, the final Born cross section is obtained in an iterative way. The efficiencies from a set of signal MC samples without any radiative correction are used to calculate a first approximation to the observed cross section. Then, by taking the observed cross sections as inputs, new MC samples are generated with radiative correction and the efficiencies as well as $(1 + \delta)$ are updated. After that, the cross sections can also be recalculated accordingly. The iterations are performed in this way until a stable result is obtained. The values of $(1 + \delta)$ from the last iteration are shown in Table I.

The term $|1 + \Pi|^2$ is the vacuum-polarization (VP) correction factor, which includes leptonic and hadronic contributions. This factor is calculated with the package provided in Ref. [50]. The package provides leptonic and hadronic VP both in the space-like and time-like regions. For the leptonic VP the complete one- and two-loop results and the known high-energy approximation for the three-loop corrections are included. The hadronic contributions are given in tabulated form in the subroutine HARD5N [51]. The $|1 + \Pi|^2$ values are also shown in Table I.

Table I and Fig. 5 show the energy dependent Born cross sections from this measurement. Taking into account the CLEO measurement at $\sqrt{s} = 4.17 \text{ GeV}$ [33], the cross section from 4.085 \sim 4.600 GeV is parameterized as the coherent sum of three Breit-Wigner (BW) functions, as shown by the solid line in Fig. 5. In the fit, the parameters of the BW around 4.36 GeV are fixed to those of the $Y(4360)$ [7] while the parameters of the other two BW functions are left free in the fit. The fitted parameters of the free BW are: $M_1 = (4204 \pm 6) \text{ MeV}/c^2$, $\Gamma_1 = (32 \pm 22) \text{ MeV}$ and $M_2 = (4496 \pm 26) \text{ MeV}/c^2$, $\Gamma_2 = (104 \pm 69) \text{ MeV}$, where the uncertainties are statistical.

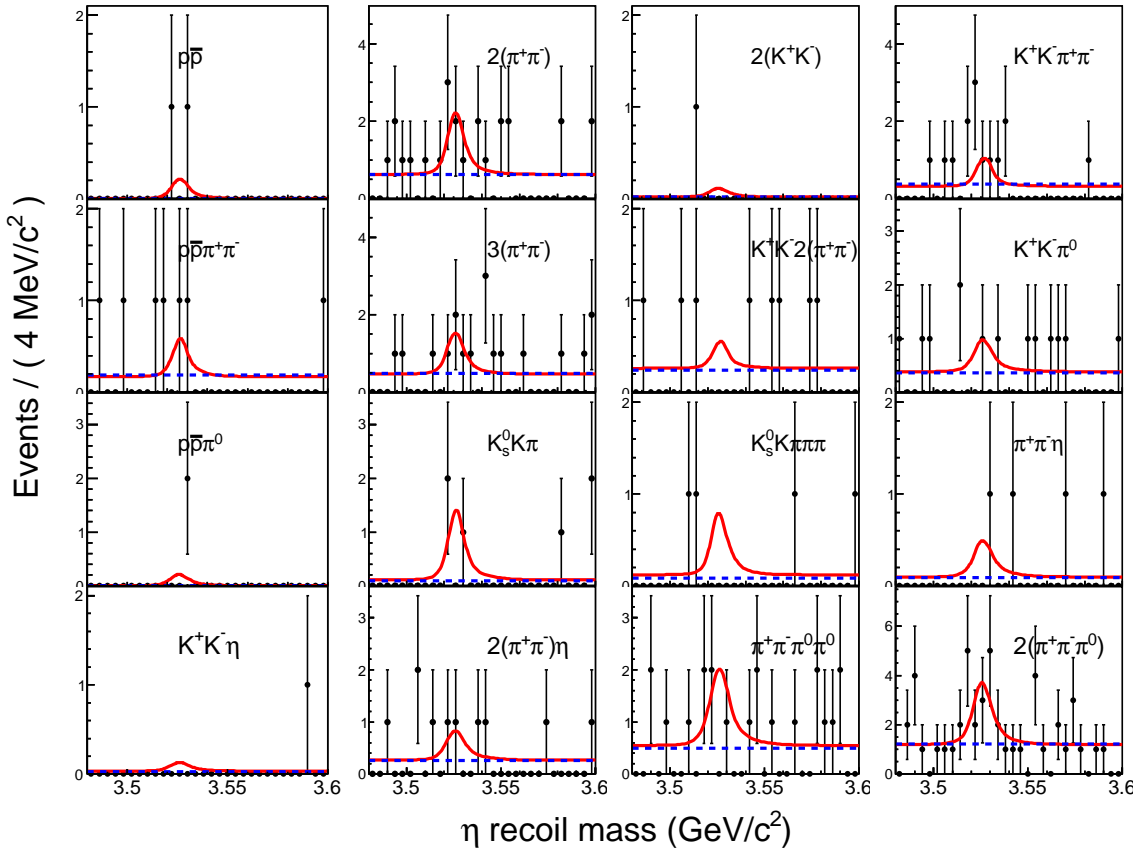


FIG. 2: Simultaneously fitted η recoil mass spectra in $e^+e^- \rightarrow \eta h_c, h_c \rightarrow \gamma \eta_c, \eta_c \rightarrow X_i$ for the 16 final states X_i at $\sqrt{s} = 4.226$ GeV. The dots with error bars represent the η recoil mass spectrum in data. The solid lines show the total fit function and the dashed lines are the background component of the fit.

VI. SYSTEMATIC UNCERTAINTIES

In this section, the study of the systematic uncertainty for the cross section measurement at $\sqrt{s} = 4.226$ GeV is described. The same method is applied to the other c.m. energies.

The main contributions to the systematic uncertainties are from the luminosity measurement, the fit method, $\mathcal{B}(h_c \rightarrow \gamma \eta_c) \mathcal{B}(\eta \rightarrow \gamma \gamma)$, ISR correction, VP correction and $\sum \epsilon_i \mathcal{B}(\eta_c \rightarrow X_i)$. The systematic uncertainties from different sources are listed in Table II. All sources are treated as uncorrelated, so the total systematic uncertainty is obtained by summing them in quadrature. The following subsections de-

scribe the procedures and assumptions that led to these estimates of the uncertainties.

A. Luminosity

The integrated luminosity is measured using Bhabha events, with an uncertainty of 1.0% [37].

B. Fit method

In the fit procedure, a discrepancy in the mass resolution between data and MC, as well as choices of background shapes and fit range introduce uncertainties on the results. Since the statistical fluctuation is large in

TABLE I: Data sets and results of the Born cross section measurement for $e^+e^- \rightarrow \eta h_c$. The table includes the integrated luminosity \mathcal{L} , the number of observed signal events N_{obs} , the radiative correction $(1 + \delta)$ and vacuum polarization correction factor $|1 + \Pi|^2$, the sum of the products of the branching fraction and efficiency $\sum \epsilon_i \mathcal{B}_i$, the Born cross section σ^B and its upper limit (at the 90% C.L.), and the statistical significance \mathcal{S} .

\sqrt{s} (MeV)	\mathcal{L} (pb $^{-1}$)	N_{obs}	$(1 + \delta)$	$ 1 + \Pi ^2$	$\sum \epsilon_i \mathcal{B}_i$ (10^{-2})	σ^B (pb)	\mathcal{S}
4085.4	52.4	$0.0_{-0}^{+1.7}$	0.68	1.052	2.40	$0.0_{-0}^{+9.4} \pm 5.4$ (< 23.7)	0.0σ
4188.6	43.1	$0.0_{-0}^{+2.9}$	0.69	1.056	2.24	$0.0_{-0}^{+20.6} \pm 13.7$ (< 52.2)	0.0σ
4207.7	54.6	$4.2_{-2.1}^{+2.4}$	0.75	1.057	2.22	$21.8_{-10.9}^{+12.5} \pm 5.7$ (< 53.6)	1.7σ
4217.1	54.1	$0.8_{-1.2}^{+2.0}$	0.85	1.057	2.18	$3.8_{-5.6}^{+9.4} \pm 1.0$ (< 32.2)	0.5σ
4226.3	1091.7	$41.2_{-8.7}^{+9.5}$	0.95	1.056	1.97	$9.5_{-2.0}^{+2.2} \pm 2.7$	5.8σ
4241.7	55.6	$0.0_{-0}^{+1.2}$	1.06	1.056	1.72	$0.0_{-0}^{+5.6} \pm 5.0$ (< 17.6)	0.0σ
4258.0	825.7	$10.3_{-5.6}^{+5.8}$	1.11	1.054	1.56	$3.4_{-1.9}^{+1.9} \pm 1.2$ (< 8.3)	2.0σ
4307.9	44.9	$0.0_{-0}^{+2.7}$	0.93	1.052	1.80	$0.0_{-0}^{+17.0} \pm 8.4$ (< 35.3)	0.0σ
4358.3	539.8	$19.0_{-5.2}^{+5.9}$	0.81	1.051	2.07	$10.0_{-2.7}^{+3.1} \pm 2.6$ (< 19.3)	4.3σ
4387.4	55.2	$0.0_{-0}^{+2.3}$	0.90	1.051	1.87	$0.0_{-0}^{+11.7} \pm 5.8$ (< 26.2)	0.0σ
4415.6	1073.6	$18.6_{-7.2}^{+7.8}$	0.94	1.053	1.65	$5.3_{-2.0}^{+2.2} \pm 1.4$ (< 11.2)	2.9σ
4467.1	109.9	$3.1_{-2.4}^{+2.1}$	0.85	1.055	1.79	$8.8_{-6.8}^{+5.9} \pm 2.3$ (< 19.0)	1.1σ
4527.1	110.0	$2.1_{-2.3}^{+2.3}$	0.94	1.055	1.38	$7.0_{-7.6}^{+7.6} \pm 1.8$ (< 27.7)	0.8σ
4574.5	47.7	$0.0_{-0}^{+1.2}$	1.15	1.055	0.88	$0.0_{-0}^{+11.8} \pm 6.8$ (< 28.6)	0.0σ
4599.5	566.9	$4.0_{-2.2}^{+3.3}$	1.27	1.055	0.75	$3.5_{-1.9}^{+2.9} \pm 0.9$ (< 11.1)	1.7σ

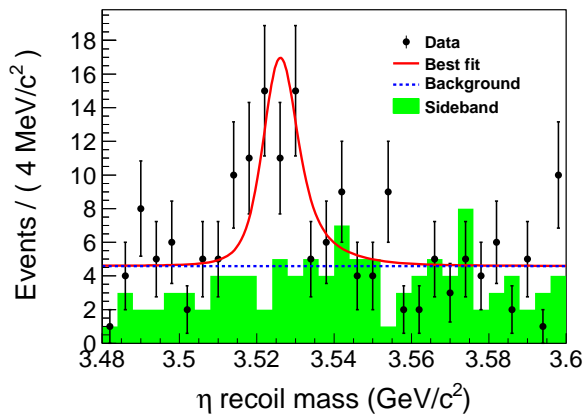


FIG. 3: Sum of the simultaneous fits to η recoil mass spectra for all 16 η_c decay modes at $\sqrt{s} = 4.226$ GeV. The dots with error bars represent the η recoil mass spectrum in data. The solid line shows the total fit function and the dashed line is the background component of the fit. The shaded histogram shows the events from the η_c sidebands.

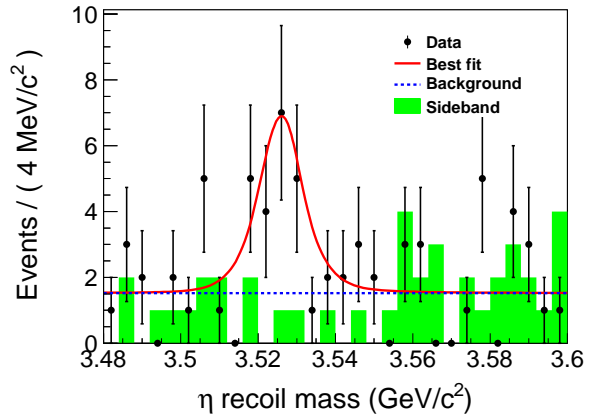


FIG. 4: Sum of the simultaneous fits to η recoil mass spectra for all 16 η_c decay modes at $\sqrt{s} = 4.358$ GeV. The dots with error bars represent the η recoil mass spectrum in data. The solid line shows the total fit function and the dashed line is the background component of the fit. The shaded histogram shows the events from η_c sidebands.

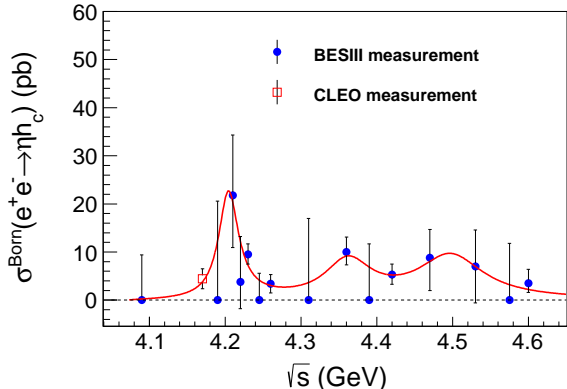


FIG. 5: Fit to the cross section of $e^+e^- \rightarrow \eta h_c$ as a function of c.m. energies. The square with error bar shows the measurement from CLEO [33], the dots with error bars refer to the results of this measurement, and the solid line shows the fit result with 3 coherent BW functions.

the data sets, we cannot obtain a stable and reasonable estimation by simply comparing two fits with different choices. To avoid the influence of statistical fluctuations, ensembles of simulated data samples (toy MC samples) are generated according to an alternative fit model with the same statistics as data, then fitted by the nominal model and the alternative model. These trials are performed 500 times, and the deviation of mean values in the two trials is taken as the systematic uncertainty. The data samples taken at $\sqrt{s} = 4.226, 4.258, 4.358,$ and 4.416 GeV are used to obtain an average uncertainty.

A discrepancy in mass resolution and mass scale between data and MC simulation affects the fit result. To estimate this uncertainty, the signal shape is smeared and shifted by convolving it with a Gaussian function with a mean value of -1.2 MeV and standard deviation of 0.04 MeV, which are obtained from the study of a control sample of $e^+e^- \rightarrow \eta J/\psi$. Toy MC samples are generated according to the smeared MC shape and fitted with a smeared and unsmeared

signal shape. The average deviation determined from the four data samples is 7.5% and is taken as systematic uncertainty.

Similarly, to estimate the uncertainty due to the background shape, a sum of signal shape and a second-order polynomial function with parameters determined from the fit on data is used to generate toy MC, then the toy MC samples are fitted by models with a first-order and a second-order polynomial background, respectively. The average deviation from the four data samples is found to be 6.3% and is taken as systematic uncertainty.

The systematic uncertainty for the fit range is determined by varying the fit ranges randomly for 400 times. The standard deviation of the fit results is taken as systematic uncertainty, which is determined to be 2.8% from the four data samples.

C. $\mathcal{B}(h_c \rightarrow \gamma \eta_c) \mathcal{B}(\eta \rightarrow \gamma \gamma)$

The branching fraction of $h_c \rightarrow \gamma \eta_c$ is taken from Ref. [52]. The uncertainty in this measurement is 15.7% and the uncertainty of $\mathcal{B}(\eta \rightarrow \gamma \gamma)$ is 0.5% [44]. These uncertainties propagate to the cross section measurement.

D. ISR correction

To obtain the ISR correction factor, the energy dependent cross section is parameterized with the sum of 3 coherent BW functions fitted to the cross sections measured in this analysis and the CLEO value at 4.17 GeV [33]. The uncertainty of the input cross section is estimated by two alternative models. First, the energy-dependent cross sections are fitted with a sum of BW and a second order polynomial function. Second, the cross sections are fitted with a second order polynomial function only. The maximum difference in ISR correction factor and detection efficiency among these hypotheses

is taken as systematic uncertainty due to the ISR correction.

E. Vacuum polarization correction

To investigate the uncertainty due to the vacuum polarization factor, we use two available VP parameterisations [50, 53]. The difference between them is 0.3% and is taken as the systematic uncertainty.

$$\mathbf{F.} \quad \sum_i \epsilon_i \mathcal{B}(\eta_c \rightarrow X_i)$$

The branching ratios $\mathcal{B}(\eta_c \rightarrow X_i)$ are taken from BESIII measurements [54], and the uncertainty of each channel is given in Table III. The systematic uncertainties associated with the efficiency include many items: tracking, photon and PID efficiency, K_S^0 , π^0 , η and η_c reconstruction, kinematic fit, cross feed and size of the MC sample. The procedure to estimate each item is described below, and the results are also listed in Table III.

- Charged track, photon reconstruction and PID efficiencies

Both the tracking and PID efficiency uncertainties for charged tracks from the interaction point are determined to be 1% per track, using the control samples of $J/\psi \rightarrow \pi^+\pi^-\pi^0$, $J/\psi \rightarrow p\bar{p}\pi^+\pi^-$ and $J/\psi \rightarrow K_S^0 K^+\pi^- + c.c.$ [55]. The uncertainty due to the reconstruction of photons is 1% per photon and it is determined from studies of $e^+e^- \rightarrow \gamma\mu^+\mu^-$ control samples [56].

- K_S^0 efficiency

The uncertainty caused by K_S^0 reconstruction is studied with the processes $J/\psi \rightarrow K^{*\pm}K^\mp$ and $J/\psi \rightarrow \phi K_S^0 K^\pm \pi^\mp$. The difference between MC simulation and data is found to

be 1.2% and is taken as systematic uncertainty.

- η/π^0 efficiency

To estimate the uncertainty due to the resolution difference in $M(\gamma\gamma)$ between data and MC simulation in the η and π^0 candidate selection, the MC shape of η (π^0) is smeared by convolving it with a Gaussian function that represents the discrepancy of resolution and is determined by the study of an $e^+e^- \rightarrow \eta J/\psi$ control sample. The difference of reconstruction efficiencies with and without smearing is taken as systematic uncertainty.

- η_c decay model

We use phase space to simulate η_c decays in our analysis. To estimate the systematic uncertainty due to neglecting intermediate states in these decays, we study the intermediate states in η_c decays from $\psi(3686) \rightarrow \gamma\eta_c, \eta_c \rightarrow X_i$ and generate MC samples accordingly. For channels with well-understood intermediate states, MC samples with these intermediate states were generated according to the relative branching ratios given by PDG [44]. The spreads of the efficiencies obtained from the phase-space and alternative MC samples are taken as the systematic uncertainties.

- η_c line shape

The uncertainties of the η_c line shape originate from the model of η_c and the errors of its resonant parameters. In the current MC generator, the η_c line shape is described by a BW function. However, in $E1$ transitions $h_c \rightarrow \gamma\eta_c$ a cubic photon energy term with a damping term at higher energies is introduced to the signal shape because of the transition matrix element and phase space factor. To estimate this

uncertainty, toy MC samples, generated according to the model that takes the $E1$ photon energy dependency into account, are analyzed to obtain the efficiency difference. The uncertainties due to the η_c resonant parameters are considered by varying m_{η_c} and Γ_{η_c} in the MC simulation within their errors given by PDG [44]. The sum of these two items added in quadrature is taken as systematic uncertainty due to the η_c line shape.

- Kinematic fit

For the signal MC samples, corrections to the track helix parameters and the corresponding covariance matrix for all charged tracks are made to obtain improved agreement between data and MC simulation [57]. The difference between the obtained efficiencies with and without this correction is taken as the systematic uncertainty due to the kinematic fit.

- Cross feed

To check the contamination among the 16 decay modes of η_c , 40,000 MC events for each channel are used to test the event misjudgement.

- Size of the MC sample

The efficiency of each channel is obtained by MC simulation. The statistical uncertainty is calculated according to a binomial distribution.

In the fit procedure, $\epsilon_i \mathcal{B}(\eta_c \rightarrow X_i) / \sum \epsilon_i \mathcal{B}(\eta_c \rightarrow X_i)$ is used to constrain the strength among different η_c decay modes, so the uncertainty from $\epsilon_i \mathcal{B}(\eta_c \rightarrow X_i)$ will affect the fit results. In this case, we cannot simply add the uncertainty from $\epsilon_i \mathcal{B}(\eta_c \rightarrow X_i)$ in quadrature with the other uncertainties. To consider the uncertainties of $\epsilon_i \mathcal{B}(\eta_c \rightarrow X_i)$ and their influence to the simultaneous fit, we change the $\epsilon_i \mathcal{B}(\eta_c \rightarrow X_i)$ within their errors and

refit the data sample. The change of the cross section with the new results is taken as systematic uncertainty.

In this procedure, systematic uncertainties are divided into two categories: the correlated part, which includes tracking, photon efficiency, PID efficiency, $\pi^0/\eta/K_S^0$ efficiency, η_c line shape and kinematic fit, and the uncorrelated part, which includes the η_c decay mode, cross feed, MC samples and $\mathcal{B}(\eta_c \rightarrow X)$. These uncertainties are assumed to be distributed according to a Gaussian distribution. The uncertainties of the correlated part are changed dependently (increasing or decreasing at the same time for all channels), while the uncertainties of the uncorrelated part are changed independently. We change the uncertainties (both correlated and uncorrelated parts) with a Gaussian constraint and refit the data set 500 times. The cross sections calculated with these trials are fitted with a Gaussian function, whose standard deviation is taken as systematic uncertainty. To obtain a conservative estimation, the maximum deviation of 16.7% from the data samples at $\sqrt{s} = 4.226, 4.258, 4.358$ and 4.416 GeV is adopted as systematic uncertainty from $\sum_i \epsilon_i \times \mathcal{B}(\eta_c \rightarrow X_i)$ for all the data sets.

TABLE II: Summary of systematic uncertainties on $\sigma^B(e^+e^- \rightarrow \eta h_c)$ (in %) at $\sqrt{s} = 4.226$ GeV.

Sources	uncertainty in σ^B (%)
Luminosity	1.0%
Signal shape	7.5%
Background shape	6.3%
Fitting range	2.8%
$\mathcal{B}(h_c \rightarrow \gamma \eta_c) \mathcal{B}(\eta \rightarrow \gamma \gamma)$	15.7%
ISR correction	13.9%
VP correction	0.3%
$\sum_i \epsilon_i \times \mathcal{B}(\eta_c \rightarrow X_i)$	16.7%
Total	28.7%

TABLE III: Systematic uncertainties (in %) for $\epsilon_i \mathcal{B}(\eta_c \rightarrow X_i)$ for each η_c exclusive decay channel.

Sources	$p\bar{p}$	$2(\pi^+\pi^-)$	$2(K^+K^-)$	$K^+K^-\pi^+\pi^-$	$p\bar{p}\pi^+\pi^-$	$3(\pi^+\pi^-)$	$K^+K^-2(\pi^+\pi^-)$	$K^+K^-\pi^0$
Tracking eff.	2.0	4.0	4.0	4.0	4.0	6.0	6.0	2.0
Photon eff.	3.0	3.0	3.0	3.0	3.0	3.0	3.0	5.0
PID	2.0	4.0	4.0	4.0	4.0	6.0	6.0	2.0
K_S^0 eff.	–	–	–	–	–	–	–	–
π^0 eff.	–	–	–	–	–	–	–	3.0
η eff.	1.7	2.0	2.6	1.7	1.7	1.7	2.0	1.3
η_c decay model	0.0	2.1	3.7	0.6	2.5	0.0	3.0	4.6
η_c line shape	6.2	6.2	6.2	6.2	6.2	6.2	5.0	5.0
Kinematic fit	2.3	3.8	3.9	3.5	3.0	6.1	4.4	1.3
Cross feed	0.0	0.7	0.0	2.0	0.0	0.0	0.0	0.0
MC sample	0.9	1.2	1.7	1.4	1.4	1.6	2.1	1.4
$\mathcal{B}(\eta_c \rightarrow X_i)$	37.0	22.0	46.0	26.0	34.0	28.0	54.0	23.0

Sources	$p\bar{p}\pi^0$	$K_S^0 K^\pm \pi^\mp$	$K_S^0 K^\pm \pi^\mp \pi^\pm \pi^\mp$	$\pi^+\pi^-\eta$	$K^+K^-\eta$	$2(\pi^+\pi^-\eta)$	$\pi^+\pi^-\pi^0\pi^0$	$2(\pi^+\pi^-\pi^0)$
Tracking eff.	2.0	4.0	6.0	2.0	2.0	4.0	2.0	4.0
Photon eff.	5.0	3.0	3.0	5.0	5.0	5.0	7.0	7.0
PID	2.0	4.0	6.0	2.0	2.0	4.0	2.0	4.0
K_S^0 eff.	–	1.2	1.2	–	–	–	–	–
π^0 eff.	2.3	–	–	–	–	–	3.1	1.5
η eff.	2.2	1.6	2.1	1.7	1.5	2.2	1.9	1.2
η_c decay model	5.8	2.5	5.2	5.5	8.1	0.0	0.1	0.5
η_c line shape	5.1	5.0	6.2	5.0	6.2	5.0	5.1	5.1
Kinematic fit	2.1	2.4	1.7	1.1	2.5	1.8	0.5	2.9
Cross feed	0.0	0.0	0.0	0.0	7.7	0.0	0.0	0.0
MC sample	1.4	1.4	2.1	1.4	1.5	1.9	1.9	2.9
$\mathcal{B}(\eta_c \rightarrow X_i)$	38.0	21.0	28.0	28.0	54.0	30.0	22.0	20.0

VII. UPPER LIMIT WITH SYSTEMATIC UNCERTAINTY

For the data sets without significant ηh_c signals observed, an upper limit at the 90% confidence level (C.L.) on the cross section is set using a Bayesian method, assuming a flat prior in σ . In this method, the probability density function of the measured cross section σ , $P(\sigma)$, is determined using a maximum likelihood fit.

The 90% confidence limit (L) is then calculated by solving the equation

$$0.1 = \int_L^\infty P(\sigma) d\sigma. \quad (3)$$

To include multiplicative systematics, $P(\sigma)$ is convolved with a probability distribution function of sensitivity, which refers to the denominator of Eq. (1) and is assumed

to be a Gaussian with central value \hat{S} and standard deviation σ_s [58]:

$$P'(\sigma) = \int_0^1 P\left(\frac{S}{\hat{S}}\sigma\right) \exp\left[\frac{-(S - \hat{S})^2}{2\sigma_s^2}\right] dS. \quad (4)$$

Here, $P(\sigma)$ is the likelihood distribution obtained from the fit and parameterized as double Gaussian. By integrating $P'(\sigma)$ we obtain the 90% C.L. upper limit taking the systematic uncertainties into account.

VIII. RESULTS AND DISCUSSION

In this study, the Born cross section and its upper limits of $e^+e^- \rightarrow \eta h_c$ are measured with statistical and systematical uncertainties at c.m. energies from 4.085 to 4.600 GeV, and the results are listed in Table I. Clear signals of $e^+e^- \rightarrow \eta h_c$ are observed at $\sqrt{s} = 4.226$ GeV for the first time. The Born cross section is measured to be $(9.5_{-2.0}^{+2.2} \pm 2.7)$ pb. We also observe evidence for the signal process at $\sqrt{s} = 4.358$ GeV with a cross section of $(10.0_{-2.7}^{+3.1} \pm 2.6)$ pb. For the other c.m. energies considered, no significant signals are found, and upper limits on the cross section at the 90% C.L. are determined.

The cross sections measured in this analysis and CLEO [33] are modeled with a coherent sum of three BW functions (as shown in Fig. 5) to calculate the ISR correction factors. Comparing with the cross section of $e^+e^- \rightarrow \pi^+\pi^-h_c$ [13], which is shown in Fig. 6, we find that the cross section at $\sqrt{s} = 4.226$ GeV is larger than that at $\sqrt{s} = 4.258$ GeV in both processes. However, due to the limited statistics, we cannot draw a clear conclusion about the production mechanism of $e^+e^- \rightarrow \eta h_c$.

Acknowledgments

The BESIII collaboration thanks the staff of BEPCII and the IHEP computing cen-

ter for their strong support. This work is supported in part by National Key Basic Research Program of China under Contract No. 2015CB856700; National Natural Science Foundation of China (NSFC) under Contracts Nos. 11235011, 11335008, 11425524, 11625523, 11635010; the Chinese Academy of Sciences (CAS) Large-Scale Scientific Facility Program; the CAS Center for Excellence in Particle Physics (CCEPP); Joint Large-Scale Scientific Facility Funds of the NSFC and CAS under Contracts Nos. U1332201, U1532257, U1532258; CAS under Contracts Nos. KJCX2-YW-N29, KJCX2-YW-N45, QYZDJ-SSW-SLH003; 100 Talents Program of CAS; National 1000 Talents Program of China; IN-PAC and Shanghai Key Laboratory for Particle Physics and Cosmology; German Research Foundation DFG under Contracts Nos. Collaborative Research Center CRC 1044, FOR 2359; Istituto Nazionale di Fisica Nucleare, Italy; Joint Large-Scale Scientific Facility Funds of the NSFC and CAS; Koninklijke Nederlandse Akademie van Wetenschappen (KNAW) under Contract No. 530-4CDP03; Ministry of Development of Turkey under Contract No. DPT2006K-120470; National Natural Science Foundation of China (NSFC) under Contract No. 11505010; National Science and Technology fund; The Swedish Research Council; U. S. Department of Energy under Contracts Nos. DE-FG02-05ER41374, DE-SC-0010118, DE-SC-0010504, DE-SC-0012069; University of Groningen (RuG) and the Helmholtzzentrum fuer Schwerionenforschung GmbH (GSI), Darmstadt; WCU Program of National Research Foundation of Korea under Contract No. R32-2008-000-10155-0.

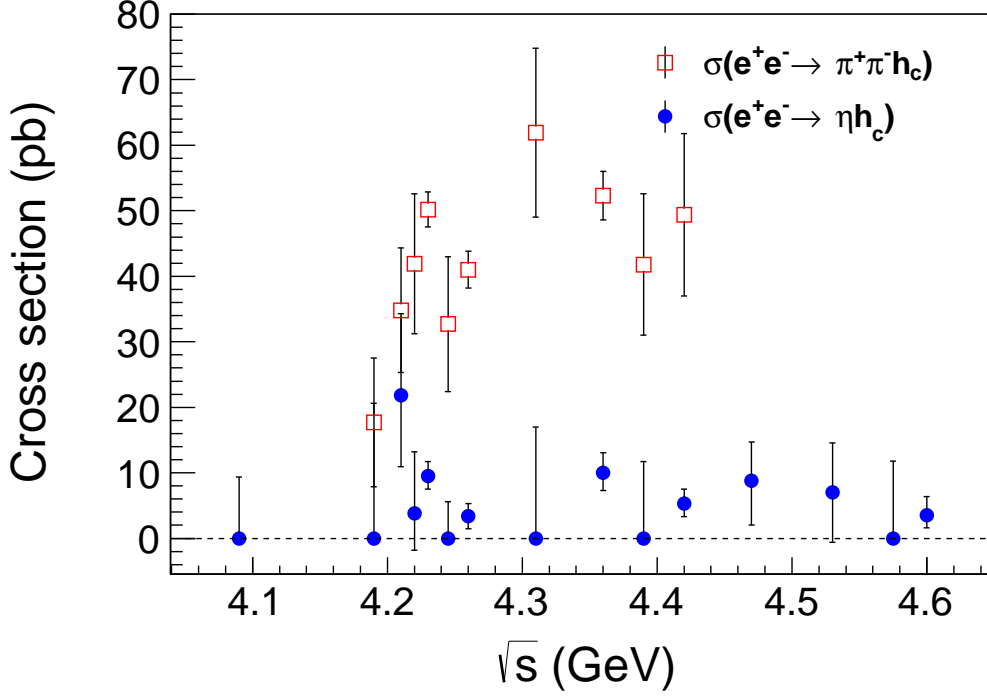


FIG. 6: Comparison between the cross sections of $e^+e^- \rightarrow \eta h_c$ (dots with error bars) and $e^+e^- \rightarrow \pi^+\pi^-h_c$ (squares with error bars) [13]. The errors are statistical only.

-
- [1] M. Ablikim *et al.* [BES Collaboration], eConf C **070805**, 02 (2007) [Phys. Lett. B **660**, 315 (2008)]; T. Barnes, S. Godfrey and E. S. Swanson, Phys. Rev. D **72**, 054026 (2005).
- [2] B. Aubert *et al.* [BaBar Collaboration], Phys. Rev. Lett. **95**, 142001 (2005).
- [3] Q. He *et al.* [CLEO Collaboration], Phys. Rev. D **74**, 091104 (2006).
- [4] C. Z. Yuan *et al.* [Belle Collaboration], Phys. Rev. Lett. **99**, 182004 (2007).
- [5] M. Ablikim *et al.* [BESIII Collaboration], Phys. Rev. Lett. **115**, 112003 (2015).
- [6] B. Aubert *et al.* [BaBar Collaboration], Phys. Rev. Lett. **98**, 212001 (2007).
- [7] X. L. Wang *et al.* [Belle Collaboration], Phys. Rev. Lett. **99**, 142002 (2007).
- [8] S. K. Choi *et al.* [Belle Collaboration], Phys. Rev. Lett. **91**, 262001 (2003).
- [9] M. Ablikim *et al.* [BESIII Collaboration], Phys. Rev. Lett. **110**, 252001 (2013).
- [10] Z. Q. Liu *et al.* [Belle Collaboration], Phys. Rev. Lett. **110**, 252002 (2013).
- [11] M. Ablikim *et al.* [BESIII Collaboration], Phys. Rev. Lett. **112**, 022001 (2014).
- [12] M. Ablikim *et al.* [BESIII Collaboration], Phys. Rev. Lett. **115**, 222002 (2015).
- [13] M. Ablikim *et al.* [BESIII Collaboration], Phys. Rev. Lett. **111**, 242001 (2013).
- [14] M. Ablikim *et al.* [BESIII Collaboration], Phys. Rev. Lett. **112**, 132001 (2014).
- [15] M. Ablikim *et al.* [BESIII Collaboration], Phys. Rev. Lett. **113**, 212002 (2014).
- [16] M. Ablikim *et al.* [BESIII Collaboration], Phys. Rev. Lett. **115**, 182002 (2015).
- [17] F. E. Close and P. R. Page, Phys. Lett. B **628**, 215 (2005).
- [18] S. -L. Zhu, Phys. Lett. B **625**, 212 (2005); E. Kou and O. Pene, Phys. Lett. B **631**, 164 (2005); X. Q. Luo and Y. Liu, Phys. Rev. D **74**, 034502 (2006) [Phys. Rev. D **74**, 039902

- (2006)].
- [19] D. Ebert, R. N. Faustov and V. O. Galkin, Phys. Lett. B **634**, 214 (2006).
- [20] L. Maiani, V. Riquer, F. Piccinini and A. D. Polosa, Phys. Rev. D **72**, 031502 (2005).
- [21] T. W. Chiu *et al.* [TWQCD Collaboration], Phys. Rev. D **73**, 094510 (2006).
- [22] X. Liu, X. -Q. Zeng and X. -Q. Li, Phys. Rev. D **72**, 054023 (2005).
- [23] C. F. Qiao, Phys. Lett. B **639**, 263 (2006).
- [24] C. Z. Yuan, P. Wang and X. H. Mo, Phys. Lett. B **634**, 399 (2006).
- [25] H.-X. Chen, L. Maiani, A. D. Polosa and V. Riquer, Eur. Phys. J. C **75**, 550 (2015).
- [26] M. Padmanath, C. B. Lang and S. Prelovsek, Phys. Rev. D **92**, 034501 (2015).
- [27] D. V. Bugg, J. Phys. G **35**, 075005 (2008).
- [28] D. Y. Chen and X. Liu, Phys. Rev. D **84**, 034032 (2011).
- [29] Q. Wang, C. Hanhart and Q. Zhao, Phys. Rev. Lett. **111**, 132003 (2013).
- [30] E. S. Swanson, Phys. Rev. D **91**, 034009 (2015).
- [31] Q. Wang, M. Cleven, F. K. Guo, C. Hanhart, U. G. Meißner, X. G. Wu and Q. Zhao, Phys. Rev. D **89**, 034001 (2014).
- [32] R. F. Lebed, R. E. Mitchell and E. S. Swanson, Prog. Part. Nucl. Phys. **93**, 143 (2017).
- [33] T. K. Pedlar *et al.* [CLEO Collaboration], Phys. Rev. Lett. **107**, 041803 (2011).
- [34] M. B. Voloshin, Phys. Lett. B **604**, 69 (2004).
- [35] M. Ablikim *et al.* [BESIII Collaboration], Phys. Rev. Lett. **118**, 092002 (2017).
- [36] U. Tamponi *et al.* [Belle Collaboration], Phys. Rev. Lett. **115**, 142001 (2015).
- [37] M. Ablikim *et al.* [BESIII Collaboration], Chin. Phys. C **39**, 093001 (2015).
- [38] M. Ablikim *et al.* [BESIII Collaboration], Chin. Phys. C **40**, 063001 (2016).
- [39] M. Ablikim *et al.* [BESIII Collaboration], Nucl. Instrum. Meth. A **614**, 345 (2010).
- [40] S. Agostinelli *et al.* [GEANT4 Collabora-
tion], Nucl. Instrum. Meth. A **506**, 250 (2003);
Geant4 version: v09-03p0; Physics List
simulation engine: BERT; Physics List en-
gine packaging library: PACK 5.5.
- [41] J. Allison *et al.*, IEEE Trans. Nucl. Sci. **53**, 270 (2006).
- [42] S. Jadach, B. F. L. Ward and Z. Was, Comp. Phys. Commun. **130**, 260 (2000); S. Jadach, B. F. L. Ward and Z. Was, Phys. Rev. D **63**, 113009 (2001).
- [43] R. G. Ping, Chin. Phys. C **32**, 599 (2008); D. J. Lange, Nucl. Instrum. Meth. A **462**, 152 (2001).
- [44] C. Patrignani *et al.* [Particle Data Group], Chin. Phys. C **40**, 100001 (2016).
- [45] J. C. Chen, G. S. Huang, X. R. Qi, D. H. Zhang and Y. S. Zhu, Phys. Rev. D **62**, 034003 (2000).
- [46] T. Sjöstrand *et al.*, Comput. Phys. Commun. **191**, 159 (2015).
- [47] M. Xu, *et al.*, Chin. Phys. C **33** (2009) 428.
- [48] G. Balossini, C. M. Carloni Calame, G. Montagna, O. Nicrosini and F. Piccinini, Nucl. Phys. B **758**, 227 (2006).
- [49] E. A. Kuraev and V. S. Fadin, Sov. J. Nucl. Phys. **41**, 466 (1985) [Yad. Fiz. **41**, 733 (1985)].
- [50] S. Eidelman and F. Jegerlehner, Z. Phys. C **67**, 585 (1995).
- [51] F. Jegerlehner, Nuovo Cim. C **034S1**, 31 (2011).
- [52] M. Ablikim *et al.* [BESIII Collaboration], Phys. Rev. Lett. **104**, 132002 (2010).
- [53] S. Actis *et al.* [Working Group on Radiative Corrections and Monte Carlo Generators for Low Energies Collaboration], Eur. Phys. J. C **66**, 585 (2010).
- [54] M. Ablikim *et al.* [BESIII Collaboration], Phys. Rev. D **86**, 092009 (2012).
- [55] M. Ablikim *et al.* [BESIII Collaboration], Phys. Rev. D **83**, 112005 (2011).
- [56] V. Prasad, C. Liu, X. Ji, W. Li, H. Liu and X. Lou, Physics **174**, 577 (2016).
- [57] M. Ablikim *et al.* [BESIII Collaboration], Phys. Rev. D **87**, 012002 (2013).

[58] K. Stenson, arXiv:physics/0605236.